Available online at www.sciencedirect.com
SCIENCE DIRECT®
Journal of Non-Crystalline Solids 351 (2005) 1995–2002
JOURNAL OF NON-CRYSTALLINE SOLIDS
www.elsevier.com/locate/jnoncrysol

Structure determination of low-alkali-content $Na_2S + B_2S_3$ glasses using neutron and synchrotron X-ray diffraction

Wenlong Yao [a], Steve W. Martin [a,*], Valeri Petkov [b]

[a] *Department of Materials Science and Engineering, Iowa State University of Science and Technology, 2220 Hoover Hall, Ames, IA 50011, USA*
[b] *Department of Physics, Central Michigan University, Mt. Pleasant, MI 48859, USA*

Received 28 September 2004; received in revised form 5 May 2005
Available online 23 June 2005

Abstract

The structures of low-alkali-content $xNa_2S + (1 - x)B_2S_3$ ($x \leqslant 0.2$) glasses have been studied by neutron and synchrotron X-ray diffraction. Similar results were obtained both in neutron and synchrotron X-ray diffraction experiments. One significant difference, however, is that with the higher resolution obtainable in the X-ray atomic distribution function data, the peak at 1.8 Å splits into two components, one at 1.8 Å and one at 1.93 Å with the addition of Na_2S to B_2S_3. The experimental total atomic distribution functions have been compared to model ones computed on the basis of structure data for crystalline counterparts of the glasses. The results provide direct structural evidence that doping B_2S_3 with Na_2S creates a large fraction of tetrahedrally coordinated borons in the glass.

PACS: 61.12.Ex; 61.10.Eq; 61.43.Fs

1. Introduction

As a strong glass-forming material, boron trisulfide (B_2S_3) makes an excellent network glass former [1]. Recent interest in thioborate and related chalcogenide glasses is due to their fast ion conducting (FIC) behavior when suitably doped with alkali sulfide (M_2S) modifier and considered as solid state electrolytes in solid state batteries [2,3]. To optimize their electrical properties, it is important to fully understand their short-range order structure and model their FIC conductivity.

The atomic arrangement in vitreous B_2S_3 (v-B_2S_3) has been previously studied by Raman spectroscopy, ^{11}B NMR and neutron diffraction. Two sharp lines in the Raman spectra of v-B_2S_3 are interpreted as arising from $B_2S_3S_{3/2}$ six-membered rings and $B_2S_2S_{2/2}$ four-membered rings [4,5]. Thus, the existence of similarities between the structure of glassy and crystalline B_2S_3 has been suggested. For reference, the structure of crystalline B_2S_3 is comprised of layers of planar $B_2S_3S_{3/2}$ and $B_2S_2S_{2/2}$ rings linked by sulfur bridges [6] as shown in Fig. 1. Neutron diffraction on v-B_2S_3 provides evidence for the existence of B_3S_3 six-membered rings in the glass [7], but no direct evidence could be found for the existence of four-membered rings in v-B_2S_3. Thus details of the atomic ordering in B_2S_3 glass are still not fully known. Similarly, ^{11}B MASS NMR experiments of v-B_2S_3 show strong evidence for ~75% of the B residing in six membered thioboroxyl rings and 25% of the B residing in isolated 'loose' trigonal units [8]. Such a structure is apparently identical to that of v-B_2O_3 where a similar fraction of boroxyl rings and loose trigonal units has also been observed in both neutron and NMR data [9,10].

* Corresponding author. Tel.: +1 515 294 0745; fax: +1 515 294 5444.
E-mail address: swmartin@iastate.edu (S.W. Martin).

0022-3093/$ - see front matter © 2005 Published by Elsevier B.V.
doi:10.1016/j.jnoncrysol.2005.05.003

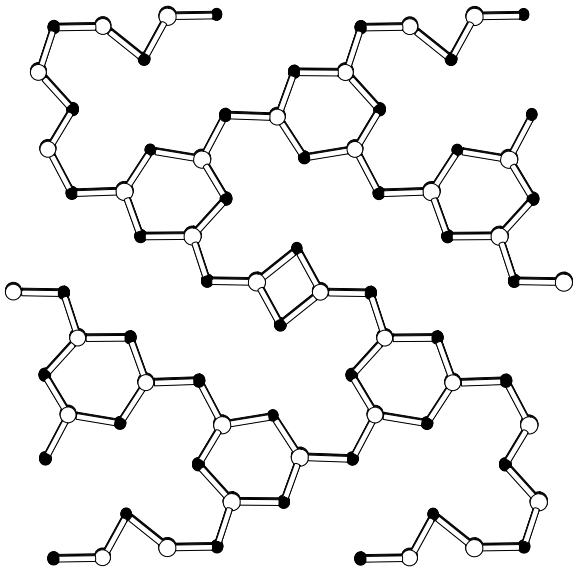

Fig. 1. Fragment of the layered structure of c-B_2S_3. Layers are made of chains of alternating four-membered $B_2S_2S_{2/2}$ and six-membered $B_2S_3S_{3/2}$ rings resulting in an average coordination number of three sulfur atoms for each boron. Boron atoms are represented as open and sulfur as solid circles.

Boron trisulfide forms binary glasses over wide composition ranges when modified by alkali sulfide [11]. Notable structural differences exist between alkali thioborate and alkali borate glasses even though they have stoichiometric similarities [12]. With the addition of alkali sulfide to boron trisulfide previous spectroscopic studies, such as infrared, Raman and NMR spectra [8,12–17], show that the overall evolution of the structure is from $BS_{3/2}$ trigonally bonded boron groups to $BS_{4/2}$ tetrahedrally bonded boron groups in the low alkali glasses ($x < 0.3$). For the high alkali glasses ($x > 0.5$), the tetrahedral boron units are then converted to trigonal boron units with increasing fractions of non-bridging sulfurs such as $MSBS_{2/2}$, $(MS)_2BS_{1/2}$ and $(MS)_3B$, where M is an alkali metal. Significant differences, however, must exist in the short range structure of the different alkali thioborate glasses because NMR studies of the composition dependence of the fraction of tetrahedral borons in these glasses show marked differences in the number of tetrahedral borons that are created per added alkali metal. In $Na_2S + B_2S_3$ glasses, for example, each added Na_2S unit is found to create ~8 tetrahedral borons compared to the stoichiometric expected value of 2 which is observed in the analogous $Na_2O + B_2O_3$ oxide glass system. Surprisingly though, as the mass of the alkali metal increases, so the formation rate of tetrahedral borons decreases; K_2S creates 4–6 tetrahedral borons, Rb_2S creates 2–3 tetrahedral borons, and finally Cs_2S creates the expected value of 2 tetrahedral borons per added alkali metal sulfide unit. While the $Li_2S + B_2S_3$ compositions phase separate in the low alkali range and therefore cannot be formed into homogenous glasses, the high alkali range glasses ($x > 0.5$) must fit this pattern because they exhibit the highest fraction of tetrahedral borons of all the alkali thioborate glasses [18]. The phase separation in the low alkali lithium thioborate glasses may be a result of the extreme formation rate of tetrahedral borons producing incompatible structures.

At this point, there appears to be little detailed understanding of why the thioborate glasses exhibit such alkali-dependent rates of formation of tetrahedral borons. One possible reason is the formation of anion complexes in the glass, such as $B_{10}S_{18}^{6-}$, where every boron is in tetrahedral coordination and a high fraction of the sulfurs exhibit 3-fold coordination [15]. A verification of this hypothesis by diffraction studies is worthwhile. However, diffraction studies on alkali modified thioborate glasses are very scarce. The only known neutron diffraction study has been performed on high alkali $xLi_2S + (1 - x)B_2S_3$ ($x > 0.5$) glasses [19].

In this paper, therefore, both neutron and synchrotron X-ray diffraction have been performed on low-alkali-content $xNa_2S + (1 - x)B_2S_3$ ($x \leqslant 0.2$) glasses where $BS_{3/2}$ units are converted to $BS_{4/2}$ units at a high conversion rate. We find direct structural evidence for the existence of such a structural transformation. A comparison between the experimental diffraction data with model ones computed from crystalline structures of similar chemical composition shows that the emerging $BS_{4/2}$ units are likely to form highly organized anion complexes.

The complimentary use of both neutron and X-ray diffraction allows us to gain insight on important details in the structure of these glasses. For example, while the B–B correlation is strong in the neutron diffraction data, these same correlations are hardly seen in the X-ray diffraction experimental data. On the other hand, the S–S correlations appear strong in the X-ray diffraction data and are much weaker in the neutron diffraction data. These differences will be used to obtain a clearer and more consistent understanding of the atomic ordering in thioborate glasses.

2. Structural determination of glasses using neutron and X-ray diffraction

The atomic-scale structure of glasses can be described in terms of atomic pair distribution functions (PDF). The widely used atomic PDF, $G(r)$, is defined as $G(r) = 4\pi r[\rho(r) - \rho_0]$, where $\rho(r)$ and ρ_0 are the local and average atomic number densities, respectively. $G(r)$ peaks at real space distances where the most frequent interatomic distances occur and thus reflects the structure of material. The stronger the disorder in a glassy material, the weaker the correlations between the positions of the atoms in it and hence, the lower the number of

Table 1
Neutron and X-ray (at $Q = 0$ Å^{-1}) weighting factors for xNa$_2$S + $(1-x)$B$_2$S$_3$ ($x \leqslant 0.2$) glasses

	B–S	B–B	S–S	Na–S	Na–B	Na–Na
B_2S_3 neutron	0.476	0.834	0.153	–	–	–
B_2S_3 X-ray	0.285	0.0297	0.685	–	–	–
0.1Na_2S neutron	0.447	0.335	0.145	0.027	0.041	0.001
0.1Na_2S X-ray	0.257	0.026	0.640	0.063	0.013	0.002
0.15Na_2S neutron	0.431	0.317	0.147	0.042	0.061	0.003
0.15Na_2S X-ray	0.243	0.024	0.617	0.094	0.019	0.004
0.2Na_2S neutron	0.414	0.298	0.144	0.056	0.081	0.006
0.2Na_2S X-ray	0.228	0.022	0.594	0.126	0.024	0.007

well-defined peaks in the PDF. Thus by obtaining an experimental atomic PDF and analyzing the location, intensity and width of peaks one can obtain information about the atomic arrangements in the glass under study. The final stage of the analysis usually involves computer simulations and comparisons between model and experimental PDF data. A structure model that reproduces well the experimental PDF data is considered to give a representative picture of the 3-D atomic arrangement in the glassy material.

Atomic PDFs can be obtained from neutron or X-ray diffraction experiments. A PDF is computed from the diffraction data via a Fourier transformation as follows:

$$G(r) = (2/\pi)\int_{Q=0}^{Q_{\max}} Q[S(Q)-1]\sin(Qr)\,\mathrm{d}Q, \tag{1}$$

where Q is the magnitude of the wave vector ($Q = 4\pi\sin\theta/\lambda$), 2θ is the angle between the incoming and outgoing radiation, λ is the wavelength of the radiation used and $S(Q)$ is the experimental total structure function. The structure function is related to the elastic part of the diffracted intensities, $I^{\mathrm{el}}(Q)$, as follows:

$$S(Q) = 1 + \left[I^{\mathrm{el}}(Q) - \sum c_i|f_i|^2\right] \Big/ \left|\sum c_i f_i\right|^2, \tag{2}$$

where c_i is the atomic concentration, and f_i is the X-ray or neutron scattering amplitude, respectively, for the atomic species of type i. For a material comprising n atomic species, a single diffraction experiment yields an atomic PDF $G(r)$ that is a weighted sum of $n(n+1)/2$ partial PDFs, $G_{ij}(r)$, each giving the spatial ordering of a particular i–j type atomic pair i.e.

$$G(r) = \sum_{i,j} w_{ij} G_{ij}(r), \tag{3}$$

where $\sum_{i,j} w_{ij} = 100\%$. Here w_{ij} are weighting factors reflecting the relative abundance and scattering power of the atomic pairs of type i–j as follows:

$$w_{ij} = c_i c_j f_i f_j \Big/ \left|\sum c_i f_i\right|^2. \tag{4}$$

Table 1 lists the neutron and X-ray weighting factors for the xNa$_2$S + $(1-x)$B$_2$S$_3$ ($x \leqslant 0.2$) glasses studied here. Both the neutron scattering lengths and the atomic form factors were obtained from Sears [20] and Hubbell [21]. As can be seen from this table, the neutron diffraction data will be expected to reflect mostly B–B and B–S atomic correlations while the X-ray diffraction data will reflect the S–S and B–S correlations. Thus employing a combination of X-ray and neutron diffraction will better reveal all of the interatomic correlations between the majority atomic species in the glasses under study.

3. Experimental

3.1. Preparation of the glasses

High purity v-B_2S_3 was synthesized in our laboratory following the method developed by Martin and Bloyer [1]. Stoichiometric amounts of amorphous boron powder (Cerac, 99.9%) and crystalline sulfur (Alfa, 99.999%) were reacted under vacuum at 800 °C in sealed, carbon-coated silica tubes in a furnace rotating at 6 rpm. ^{11}B is used in the neutron scattering experiment since ^{10}B has a large neutron absorption. For this reason, isotopically enriched ^{11}B powder (Eagle-Picher, 99.51% ^{11}B) instead of naturally abundant boron powder was used to prepare v-$^{11}B_2S_3$.

The xNa$_2$S + $(1-x)^{11}$B$_2$S$_3$ ($x \leqslant 0.2$) glasses were prepared by melting stoichiometric amounts of Na_2S and B_2S_3 at 850 °C for ~10–15 min in vitreous carbon crucibles in a high-quality O_2- and H_2O-free (<10 ppm) glove box. The melt was quenched to room temperature between brass plates.

3.2. Neutron diffraction experiments

Time-of-flight neutron diffraction experiments were performed at room temperature. Powdered xNa$_2$S + $(1-x)^{11}$B$_2$S$_3$ ($x = 0$, 0.1, 0.15 and 0.2) glasses were sealed in cylindrical vanadium containers and measured on the GLAD diffractometer at the intense pulsed neutron source (IPNS) at the Argonne National Laboratory. The data analysis followed standard procedures and included corrections for the background, scattering from the containers, absorption, multiple scattering, inelasticity effects and incoherent scattering. The back-

ground, a standard vanadium rod, and the empty vanadium sample container were also measured to enable these corrections. It was found that there was about 1% hydrogen in the glass samples presumably in the form of B–S–H groups due to the hygroscopic character of B_2S_3. Because of the large incoherent scattering cross-section of hydrogen, a standard method of hydrogen correction was performed. These were performed using the ATLAS software package for time-of-flight neutron diffraction data [22].

3.3. Synchrotron X-ray diffraction experiments

Synchrotron X-ray diffraction experiments were carried out at the BESSRC-CAT 11-ID-C beam line at the advanced photon source (APS) at the Argonne National Laboratory. Three samples $x\mathrm{Na_2S} + (1-x)\mathrm{B_2S_3}$ ($x = 0$, 0.15, and 0.2) sealed in thin glass capillaries were measured. The measurements were done with X-rays of energy 114.67 keV ($\lambda = 0.1081$ Å^{-1}). The higher energy X-rays were used to extend the range of diffraction data to higher wave vectors Q, which is important to obtain improved resolution in the real-space of atomic PDF analysis, especially at short distances. Also, it helped reduce some unwanted experimental artifacts such as absorption and multiple scattering. Scattered radiation was collected with an intrinsic germanium detector coupled to a multi-channel analyzer. Several runs were conducted and the resulting scattering data were averaged to improve the statistical accuracy and to reduce any systematic effect due to instabilities in the experimental setup. The experimental diffraction data were subjected to appropriate corrections for flux, background, Compton scattering, and sample absorption using the program RAD [23].

4. Results

4.1. Structure data from neutron diffraction

Fig. 2 shows the reduced neutron structure function $Q[S(Q)-1]$ for the four different compositions of $\mathrm{Na_2S} + \mathrm{B_2S_3}$ glasses that were studied. Although each data set was collected for ~12 h, the reduced structure functions appear somewhat noisy due to the relatively low flux of neutrons and the low scattering power of the samples. Also, although neutron diffraction data was collected to wave vectors as high as 40 Å^{-1}, the noise rendered the data above wave vectors of 16 Å^{-1} unusable. This resulted in appreciable termination ripples in the corresponding atomic distribution functions. Nevertheless, as will be shown below, the neutron diffraction data are of sufficient quality to reveal the details in the atomic ordering in the studied glasses.

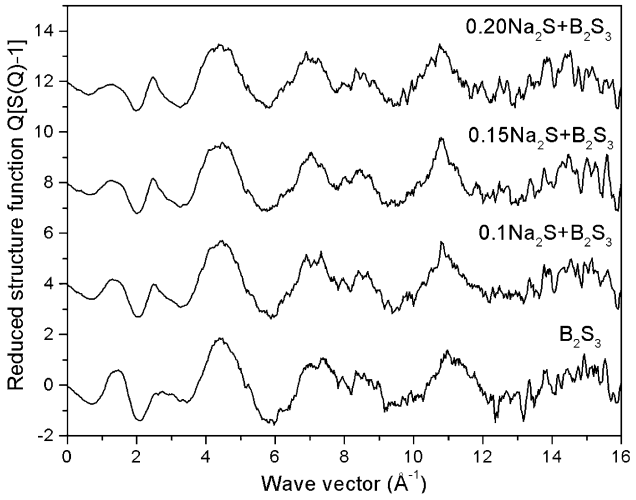

Fig. 2. Neutron reduced structure functions $Q[S(Q)-1]$ for $x\mathrm{Na_2S} + (1-x)\mathrm{B_2S_3}$ ($x \leqslant 0.2$) glasses (the curves have been offset for clarity).

The general features of the experimental data for the four glasses are fairly similar with the differences being mostly in the first peak at about 1.3 Å^{-1}, which is the so-called first sharp diffraction peak (FSDP). The FSDP changes greatly with the increase of Na_2S content, decreasing in intensity and shifting slightly to lower Q. The FSDP is regarded as a signature of medium-range order (MRO) in amorphous solids and its appearance in these glasses suggests that the addition of Na_2S significantly modifies the MRO in the B_2S_3 network [24]. Such trends in the FSDP with composition have also been reported previously in other glasses [25–27].

4.2. Atomic PDF function G(r) from neutron diffraction

The structure functions of Fig. 2 were Fourier transformed to give the atomic pair distribution functions (PDF, $G(r)$) using a Lorch modification function with $Q_{max} = 16$ Å^{-1}, and are shown in Fig. 3 for all glasses studied. With increasing Na_2S contents, the intensity and position of peaks change slightly.

The peak at 1.83 Å is assigned to the B–S correlation in trigonally bonded $BS_{3/2}$ boron groups. This value is close to the first B–S distance in c-B_2S_3, where the first B–S distance varies between 1.778 Å and 1.838 Å in both $B_2S_2S_{2/2}$ four-membered and $B_2S_3S_{3/2}$ six-membered rings, respectively [6]. Also, this distance is very close to that obtained from previous neutron diffraction for pure v-B_2S_3 and $Li_2S + B_2S_3$ glasses [7,19]. With the addition of Na_2S, the first B–S correlation shits slightly to larger distances. This may be due to the conversion from trigonally coordinated boron units to tetrahedrally coordinated boron units. The B–S distance in tetrahedrally bonded boron groups is found to vary between 1.879 Å and 1.951 Å [28]. Hence, the observed shift in

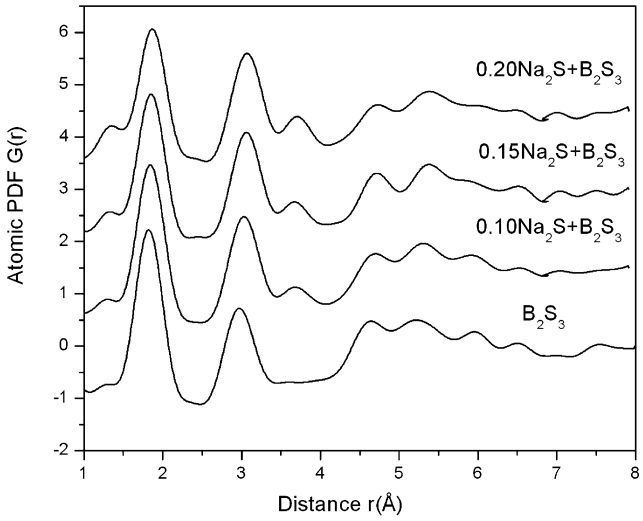

Fig. 3. Neutron atomic PDF functions $G(r)$ for $x\mathrm{Na_2S} + (1-x)\mathrm{B_2S_3}$ ($x \leqslant 0.2$) glasses (the curves have been offset for clarity).

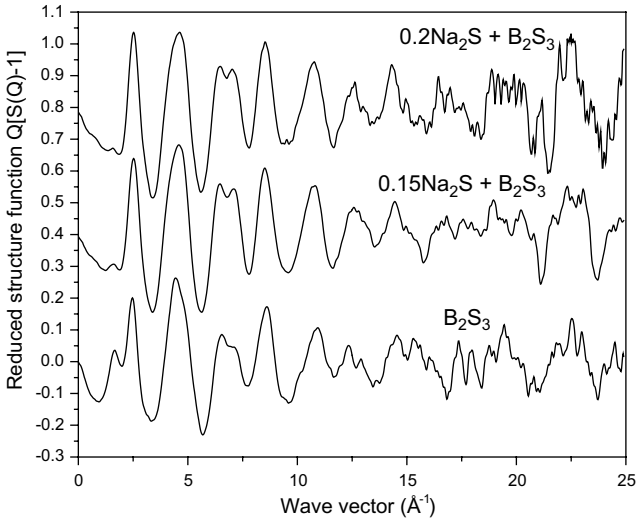

Fig. 4. Synchrotron X-ray reduced structure functions for $x\mathrm{Na_2S} + (1-x)\mathrm{B_2S_3}$ ($x \leqslant 0.2$) glasses (the curves have been offset for clarity).

the first PDF peak is consistent with the formation of tetrahedral borons in these low alkali glasses.

The peak at 2.98 Å, attributed to both B–B and S–S correlations, cannot be resolved because of their similar weighting factors and distances. The B–B distance in six-membered rings in the crystalline form of B_2S_3 is 2.94 Å and S–S distance varies between 3.06 Å and 3.26 Å [6]. Table 1 shows that the weighting for the S–S distance is relative low, but with the increase of Na_2S, the relative weighting for the S–S correlation increases. This is reflected in the neutron data where the peak shifts slightly to larger distances.

It should be mentioned that the first PDF peak shows a low-r shoulder at a distance at 1.37 Å. The shoulder may arise from a small amount of B–O correlations coming from contamination of the commercial Na_2S with oxygen. The B–O bond length is identified as being 1.37–1.38 Å in previous studies of B_2O_3 glasses [29].

4.3. Structure data from synchrotron X-ray diffraction

Fig. 4 shows the X-ray experimental reduced structure function for B_2S_3 glass and B_2S_3 glasses doped with Na_2S. The structure functions show noticeable oscillations up to the wave vector of 25 Å^{-1} achieved in the present experiments. Like the neutron data, a careful inspection of the structure functions presented in Fig. 4 shows that the first peak undergoes a dramatic change with Na_2S content: it is seen at $\sim$2 Å^{-1} in pure B_2S_3 and almost ceases to exist in the $0.20\mathrm{Na_2S} + 0.80\mathrm{B_2S_3}$ glass. This observation indicates that a considerable change in the immediate range atomic order occurs as Na_2S enters the B_2S_3 network. This trend agrees well with that of the present neutron and previous results [25–27]. The higher-Q peaks in the experimental structure factors are also seen to change with Na_2S content, although the change is not so dramatic as it is with the FSDP in $Q[S(Q)-1]$. The changes in the high-Q peaks suggest that the immediate atomic ordering, including the first neighbor atomic coordination, also experiences changes with Na_2S content.

4.4. Atomic PDF function G(r) from synchrotron X-ray diffraction

The PDF functions from synchrotron X-ray diffraction, $G(r)$, were obtained by Fourier transforming $Q[S(Q)-1]$ with $Q_{\max} = 25$ Å and are shown in Fig. 5. It should be noted that the significant difference between the neutron and X-ray results is that the peak assigned to B–S correlation splits into two components

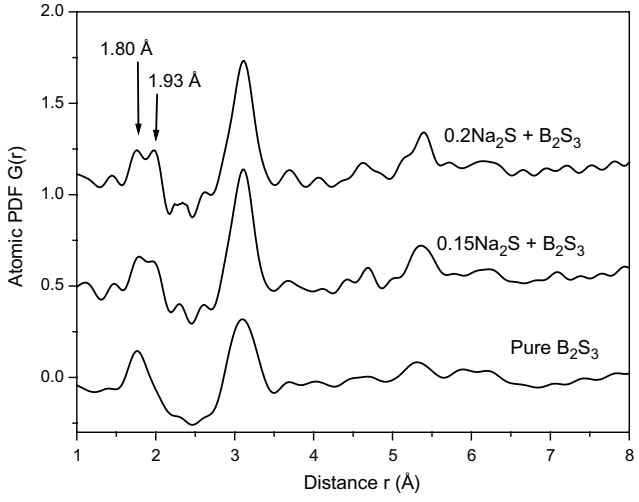

Fig. 5. Synchrotron X-ray atomic PDFs functions $G(r)$ for $x\mathrm{Na_2S} + (1-x)\mathrm{B_2S_3}$ ($x \leqslant 0.2$) glasses (the curves have been offset for clarity).

at 1.8 Å and 1.93 Å, respectively, for the two glasses containing Na_2S. Because the neutron data were collected only over a range of out to 16 $Å^{-1}$, whereas the X-ray data extend up to 25 $Å^{-1}$, the larger Q_{max} used in Fourier transformation of the X-ray diffraction data allows greater resolution in X-ray diffraction PDFs. This in turn suggests that more local structure information in the glasses can be obtained from the X-ray data.

Similar to the neutron data, the B–O correlation peak at 1.4 Å is observed and increases with the addition of Na_2S. For pure B_2S_3, the peak at 1.8 Å can be assigned to the B–S correlation in trigonally coordinated borons. With the addition of Na_2S, this peak splits into two components at 1.8 Å and 1.93 Å, respectively. The peak at the slightly longer distance of 1.93 Å is assigned to the B–S correlation in tetrahedrally coordinated $BS_{4/2}$ units. In the crystal $Na_6B_{10}S_{18}$, the B–S distance in tetrahedral coordinated boron structure is found to lie between 1.879 Å and 1.951 Å [28]. The peak at 3.1 Å is attributed mostly to S–S correlations since the weighting factor for S–S (0.6) is much larger than that of B–B (0.02), as shown in Table 1.

5. Discussion

In the study of the short-range structure of glasses, it is often found that both the glass and the crystal share similar structural units because the short-range order is dominated by bond strength and atomic size packing features of the atoms and/or ions in the material. The similarities between the short-range atomic ordering in glasses and the corresponding crystals were first pointed out by Zachariasen in a study of the silicate glasses [30]. Since, however, glasses lack the 3-D order of crystals, the structures of glasses and corresponding crystals usually disagree substantially at longer range real space distances. For example, while the structure of both v-B_2O_3 and c-B_2O_3 are built up from trigonal $BO_{3/2}$ unit with approximately the same B–O distances and O–B–O bond angles, v-B_2O_3 is observed to have significant ordering at the intermediate range to form the well-known 6-membered boroxol B_3O_3 rings, whereas c-B_2O_3 does not possess any such rings [31]. In a similar way, the structure of c-B_2S_3 crystal has been studied by Diercks and Krebs [6] and they suggest that the structure of c-B_2S_3 is comprised of a stack of layers made of four-membered B_2S_2 rings bridged to six-membered B_3S_3 rings as shown in Fig. 1.

A model atomic PDF of c-B_2S_3 calculated on the basis of this structure is compared to the experimental X-ray PDF for B_2S_3 glass in Fig. 6. As can be seen in Fig. 6, the model and experimental PDF data are similar to each other for short interatomic distances including the first near neighbor B–S (~1.8 Å) and S–S (~3.1 Å) atomic separations. This similarity suggests that the short range atomic ordering in both the crystal and the glass share similar features, i.e. they are built with the $BS_{3/2}$ unit with similar B–S distances and S–B–S angles. The model and experimental PDF data, however, disagree at longer (intermediate range) real space distances, in particular beginning around 4 Å. The model PDF shows a strong peak at ~4 Å reflecting the presence of the repeating layers in the crystal. There is no such a strong peak in the experimental PDF suggesting that B_2S_3 glass does not have the layered structure of the corresponding crystal as might be expected from its three dimensional disordered structure.

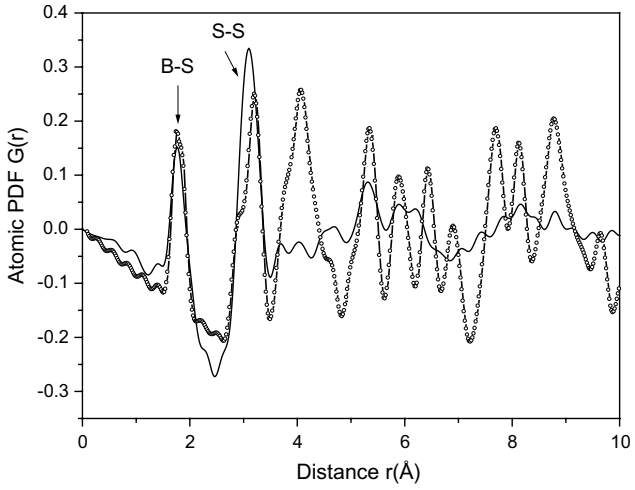

Fig. 6. Comparison between calculated model (symbols) and experimental data (line) PDFs for B_2S_3 glass. The model PDF is based on the structure of crystalline B_2S_3 shown in Fig. 1. First neighbor B–S and S–S atomic pairs are marked with arrows.

With the addition of Na_2S as a glass modifier to B_2S_3, the structure of the glasses changes in significant way. NMR, IR and Raman spectroscopic studies have shown that as in the alkali borate glasses, tetrahedrally bonded boron groups, $BS_{4/2}$, are formed with added modifier [8,12–17]. However, unlike the alkali borate glasses as described above, these $BS_{4/2}$ groups form at an extraordinary, 'super-stoichiometric' rate. The $Na_2S + B_2S_3$ glasses have the highest conversion rate (approximately eight tetrahedral groups for every added Na_2S) of the alkali thioborate glasses. This compares to the alkali borate glasses where the stoichiometric rate of two tetrahedral boron groups form for every added alkali oxide independent of the alkali. One possible structure which incorporates large fractions of $BS_{4/2}$ units in alkali thioborate systems is comprised of a pyramidal arrangement of $BS_{4/2}$ units with trigonally coordinated sulfur atoms and six-membered ring groups around the outer edges and was proposed by zum Hebel et al. [32]. This structure is found in the compound $Na_6B_{10}S_{18}$ ($3Na_2S + 5B_2S_3$, $x = 0.375$) and is reproduced in Fig. 7(c) [28]. A formation mechanism for this structure from trigonal $BS_{3/2}$ to B_3S_3 units as proposed by Conrad and

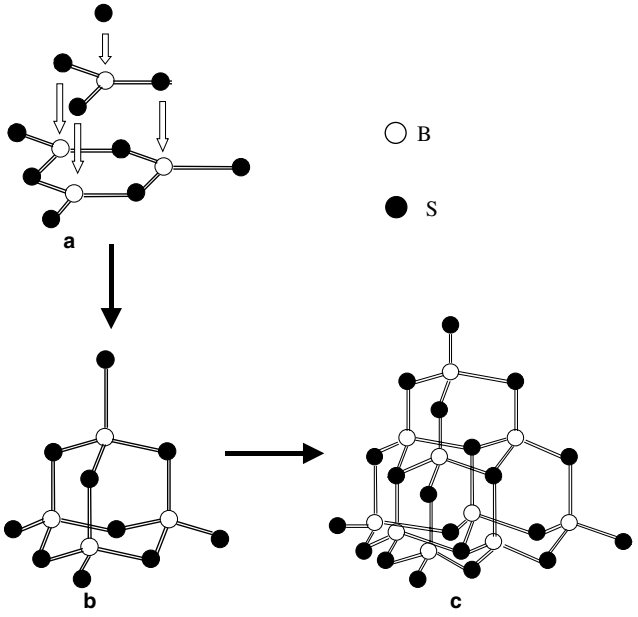

Fig. 7. Formation of B_4S_{10} and $B_{10}S_{20}$ macrotetrahedra from $BS_{3/2}$ and $B_2S_3S_{3/2}$ groups as redrawn from Ref. [33].

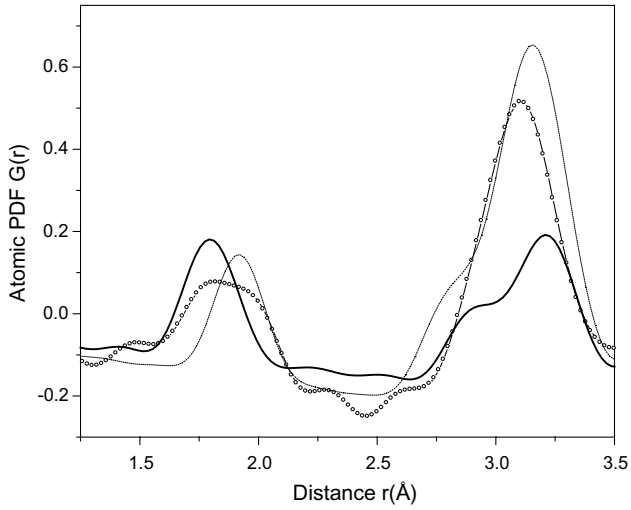

Fig. 8. Comparison between the experimental PDF for $0.15Na_2S + B_2S_3$ glass (symbols) and model PDFs for crystalline B_2S_3 (solid line) and crystalline $Na_6B_{10}S_{18}$ (broken line).

Krebs is shown in Fig. 7 [33]. First, with just one additional sulfide (from M_2S) and one planar B_3S_3 boron–sulfur unit, a B_4S_{10} macrotetrahedral unit can be formed. In a similar way, a $B_{10}S_{18}$ unit can be formed from the addition of two more B_3S_3 units to one B_4S_{10} unit.

To help understand the structure of the alkali modified glasses, we have compared the experimental PDF of the $0.15Na_2S + 0.85B_2S_3$ glass with model ones created from the known structures of crystalline B_2S_3 and $Na_6B_{10}S_{18}$, where boron atoms adopt trigonal and tetrahedral coordinations, respectively. The comparison is given in Fig. 8. As can be seen the first peak in the model PDF for crystalline B_2S_3 is positioned at ~1.8 Å, which is the B–S distance with trigonally coordinated boron. The first peak in the model PDF of crystalline $Na_6B_{10}S_{18}$ is positioned at ~1.93 Å and is the B–S distance with tetrahedrally coordinated boron. These first peaks of the model PDFs agree very well with the two components (trigonal and tetrahedral borons) of the first peak in the experimental PDFs. It is reasonable to assume therefore that the boron atoms in the $0.15Na_2S + 0.85B_2S_3$ and $0.20Na_2S + 0.80B_2S_3$ glasses are both 3-fold and 4-fold coordinated by sulfur atoms. As can be seen in Fig. 8, the second peak in the PDF of the glass (at ~3.1 Å) is better matched by the model PDF based on $Na_6B_{10}S_{18}$ structure. However, the number of close S–S correlations (across $BS_{4/2}$ tetrahedral edges) in the $Na_6B_{10}S_{18}$ crystal is much larger than the S–S correlations observed in crystalline B_2S_3. Obviously, the emerging tetrahedrally coordinated borons are accompanied by the creation of a large number of S–S correlations. Such a profound change in the immediate atomic ordering would inevitably involve a restructuring of the glassy network at longer-range distances as reflected by the dramatic change in the first sharp diffraction peak in the $S(Q)$ data. A fragment of $Na_6B_{10}S_{18}$ structure showing the B–S tetrahedral units of the type that are likely to occur in $Na_2S + B_2S_3$ glasses is shown in Fig. 7(c).

6. Conclusions

Neutron and synchrotron X-ray diffraction experiments have been performed on $xNa_2S + (1 - x)B_2S_3$ ($x \leqslant 0.2$) glasses at room temperature. Systematic changes were observed in the FSDP with the increase of Na_2S content, and these suggest that there are changes in the degree of medium-range order. Both X-ray and neutron diffraction results provide the nearest neighbor atomic correlations in the atomic PDF functions $G(r)$. Similar atom–atom distances were obtained both in the neutron and X-ray experiments. The significant difference is that in the X-ray diffraction data, the peak at 1.8 Å splits into two components, one at 1.8 Å and one at 1.93 Å, with the addition of Na_2S content. This result shows that the coordination of boron atoms undergoes transformation from trigonal to tetrahedral. Results of our diffraction and modeling studies provide direct structural evidence that doping B_2S_3 with Na_2S creates a large number of tetrahedrally coordinated boron and S–S pairs in the glass. It is likely that a structure of a pyramidal arrangement of BS_4 units, which is found in $Na_6B_{10}S_{18}$ polycrystalline, also occurs in $Na_2S + B_2S_3$ glasses.

Acknowledgments

This work was supported in part by NSF through grants DMR-9972466 and DMR-0304391. This work has benefited from the use of the Intense Pulsed Neutron Source and the Advanced Photon Source at Argonne National Laboratory. Thanks are given to J. Siewenie and Q. Mei from IPNS for the assistance with neutron experiments. M. Beno and Y. Ren from APS are thanked for the help with X-ray experiments. Use of both facilities was supported by the US Department of Energy, Office of Science, Office of Basic Energy Sciences, under Contract No. W-31-109-Eng-38.

References

[1] S.W. Martin, D.R. Bloyer, J. Am. Ceram. Soc. 73 (1990) 3481.
[2] A. Pradel, M. Ribes, Mater. Sci. Eng. B 3 (1989) 45.
[3] J. Kincs, S.W. Martin, Phys. Rev. Lett. 76 (1996) 70.
[4] A.E. Geissberger, F.L. Galeener, in: P.H. Gaskell, J.M. Parker, E.A. Davis (Eds.), The structure of non-crystalline materials, 1982, Taylor and Francis, London, 1983, p. 381.
[5] M. Menetrier, A. Hojjaji, A. Lavasseur, M. Couzi, K.J. Rao, Phys. Chem. Glasses 33 (1992) 222.
[6] H. Dietcks, B. Krebs, Angew. Chem. Int. Ed. Engl. 16 (1977) 313.
[7] R.N. Sinclair, C.E. Stone, A.C. Wright, S.W. Martin, M.L. Royle, A.C. Hannon, J. Non-Cryst. Solids 293–295 (2001) 383.
[8] S.-J. Hwang, C. Fernandez, J.P. Amoureux, J.-W. Han, J. Cho, S.W. Martin, M. Pruski, J. Am. Chem. Soc. 120 (1998) 7337.
[9] R.N. Sinclair, C.E. Stone, A.C. Wright, I.G. Polyakova, N.M. Vedishcheva, B.A. Shakhmatkin, S.A. Feller, B.C. Johanson, P. Venhuizen, R.B. Williams, A.C. Hannon, Phys. Chem. Glasses 41 (2000) 286.
[10] J.W. Zwanziger, R.E. Youngman, M. Braun, Borate glasses, crystals and melts, in: Proceedings of the International Conference on Borate Glasses, Crystals and Melts, 2nd Ed., 22–25 July 1996, Abingdon, UK, 1997, p. 21.
[11] J. Cho, PhD thesis, Iowa State University, 1995.
[12] J.A. Sills, S.W. Martin, D.R. Torgeson, J. Non-Cryst. Solids 194 (1996) 260.
[13] D.R. Bloyer, J. Cho, S.W. Martin, J. Am. Ceram. Soc. 76 (11) (1993) 2753.
[14] J. Cho, S.W. Martin, J. Non-Cryst. Solids 182 (1995) 248.
[15] M. Royle, J. Cho, S.W. Martin, J. Non-Cryst. Solids 279 (2001) 97.
[16] J.A. Sills, S.W. Martin, D.R. Torgeson, J. Non-Cryst. Solids 168 (1994) 86.
[17] J. Cho, S.W. Martin, B. Meyer, K.-H. Kim, D.R. Torgeson, J. Non-Cryst. Solids 270 (2000) 205.
[18] K.S. Suh, A. Hojjaji, G. Villeneuve, M. Menetrier, A.J. Levasseur, J. Non-Cryst. Solids 128 (1) (1991) 13.
[19] C. Estournes, A.P. Owens, M. Menetrier, A. Levasseur, K.J. Rao, S.R. Elliott, J. Non-Cryst. Solids 171 (1994) 80.
[20] V.F. Sears, Neutron News 3 (1992) 26.
[21] J.H. Hubbell, W.J. Veigele, E.A. Briggs, R.J. Howerton, J. Phys. Chem. Ref. Data 4 (1973) 471.
[22] A.K. Soper, W.S. Howells, A.C. Hannon, Rutherford Appleton Laboratory Report, 1989, p. 89-046.
[23] V. Petkov, J. Appl. Cryst. 22 (1989) 387.
[24] S.R. Elliott, J. Phys: Condens. Matter. 4 (1992) 7661.
[25] M. Misawa, D.L. Price, K. Suzuki, J. Non-Cryst. Solids 37 (1980) 85.
[26] R.J. Dejus, S. Susman, K.J. Volin, D.G. Montague, D.L. Price, J. Non-Cryst. Solids 143 (1992) 162.
[27] J.H. Lee, A.P. Owens, A. Pradel, A.C. Hannon, M. Ribes, S.R. Elliott, Phys. Rev. B 54 (1996) 3895.
[28] A. Hammerschmidt, P. zum Hebel, F. Hilttmann, B. Krebs, Z. Anorg. Allg. Chem. 622 (1996) 76.
[29] M. Misawa, J. Non-Cryst. Solids 122 (1990) 33.
[30] W.H. Zachariasen, J. Am. Chem. Soc. 54 (1932) 3841.
[31] R.L. Mozzi, B.E. Warren, J. Appl. Cryst. 3 (1970) 251.
[32] P. zum Hebel, B. Krebs, M. Grune, W. Muller-Warmuth, Solid State Ion. 43 (1990) 133.
[33] O. Conrad, B. Krebs, Phosphorus, Sulfur and Silicon 124&125 (1997) 37.